EXPERIMENTAL AEROTHERMODYNAMIC RESEARCH OF HYPERSONIC AIRCRAFT

Technical Progress Report (Substitution)

for the period
March 1, 1987 - September 30, 1987

Submitted to

National Aeronautics and Space Administration
Ames Research Center
Moffett Field, California 94035

Aerothermodynamics Branch
George S. Deiwert, Chief
William K. Lochman, Technical Monitor

NASA-Cooperative Agreement NCC2-416

Prepared by

ELORET INSTITUTE
1178 Maraschino Drive
Sunnyvale, CA 94087
Phone: (408) 730-8422 and (415) 493-4710
Telex: (ESL) 62 44 2780
K. Heinemann, President and Grant Administrator
Joseph W. Cleary, Principal Investigator
9 December, 1987

FLOW-VISUALIZATION RESULTS FOR AN ALL-BODY HYPERSONIC AIRCRAFT (U)

William K. Lockman
NASA Ames Research Center
Moffett Field, California

Scott L. Lawrence
NASA Ames Research Center
Moffett Field, California

Joseph W. Cleary
Eloret Institute
Palo Alto, California

Third National Aero-Space Plane
Technology Symposium
June 2-4, 1987

Paper Number 6

AMES ALL-BODY HYPERSONIC TEST PROGRAM FOR CFD CODE VALIDATION (U)

(U) The 2-D and 3-D advanced computer codes being developed for use in the design of such hypersonic aircraft as the National Aero-Space Plane require comparisons of the computational results with a broad spectrum of experimental data to fully assess the validity of the codes. This is particularly true for complex flow fields with control surfaces present and for flows with separation, such as leeside flow.

(U) Therefore, the objective of this ongoing investigation is to provide a hypersonic experimental data base required for validation of advanced computational fluid dynamics (CFD) computer codes and for development of more thorough understanding of the flow physics necessary for these codes. This is being done by implementing a comprehensive test program for a generic all-body hypersonic aircraft model in the NASA/Ames 3.5-foot Hypersonic Wind Tunnel over a broad range of test conditions to obtain pertinent surface and flow-field data. Results from the flow-visualization portion of the investigation will be presented in this paper.

AMES ALL–BODY HYPERSONIC TEST PROGRAM
FOR CFD CODE VALIDATION (U)

(U) OBJECTIVE: PROVIDE HYPERSONIC EXPERIMENTAL DATA BASE REQUIRED FOR
- Validation of Advanced CFD Computer Codes
- Development of More Thorough Understanding of Flow Physics Necessary for These Codes

(U) MOTIVATION: NEED FOR EXTENSIVE HYPERSONIC DATA TO FULLY VALIDATE CFD CODES TO BE USED FOR NASP & OTHER HYPERSONIC VEHICLES

(U) APPROACH: IMPLEMENT COMPREHENSIVE TEST PROGRAM IN AMES 3.5–FT HWT TO OBTAIN PERTINENT SURFACE & FLOW–FIELD DATA FOR GENERIC ALL–BODY MODEL OVER BROAD RANGE OF TEST CONDITIONS

6–1

AMES ALL-BODY HYPERSONIC AIRCRAFT EXPERIMENT (U)
AMES 3.5-FT HWT (U)

(U) The all-body hypersonic aircraft model will be described and shown in the next four figures. The all-body model is representative of a hypersonic cruise vehicle derived from the analytical studies of references 1 to 4. The aerodynamic characteristics of this configuration were previously investigated from subsonic to hypersonic Mach numbers (ref. 5). The present pressure model is larger than the force model of reference 5 (36- versus 19-in. model length). The all-body model has a delta planform with leading-edge sweepback of 75°. The forebody is an elliptic cone with a major-to-minor axis ratio of 4 and the afterbody has elliptical cross sections with a sharp straight-line trailing edge. This relatively simple model geometry can be easily gridded for CFD codes. The model can be tested with a sharp or blunt nose tip and without or with control surfaces (combination horizontal/vertical tails). The canard will not be used for this hypersonic test program.

AMES ALL–BODY HYPERSONIC AIRCRAFT EXPERIMENT (U)
AMES 3.5–FT HWT (U)

(U) MODEL:

(U) AMES GENERIC ALL–BODY HYPERSONIC AIRCRAFT

- Delta Planform ($\Lambda = 75°$)
  - Forebody – Elliptic Cone (a/b = 4)
  - Afterbody – Elliptical Cross Sections with Sharp Trailing Edge
- Sharp or Blunt Nose Tip
- With or Without Control Surfaces
  - Canard (Not Used)
  - Combination Horizontal/Vertical Tails

AMES ALL-BODY HYPERSONIC AIRCRAFT MODEL (U)
WITH CONTROL SURFACES (U)

(U) This is a photograph of the complete all-body model with control surfaces (canard and combination horizontal/vertical tails). The support sting for mounting the model in the tunnel is attached to the model along the afterbody centerline.

ALL–BODY HYPERSONIC AIRCRAFT MODEL (U)
WITH CONTROL SURFACES (U)

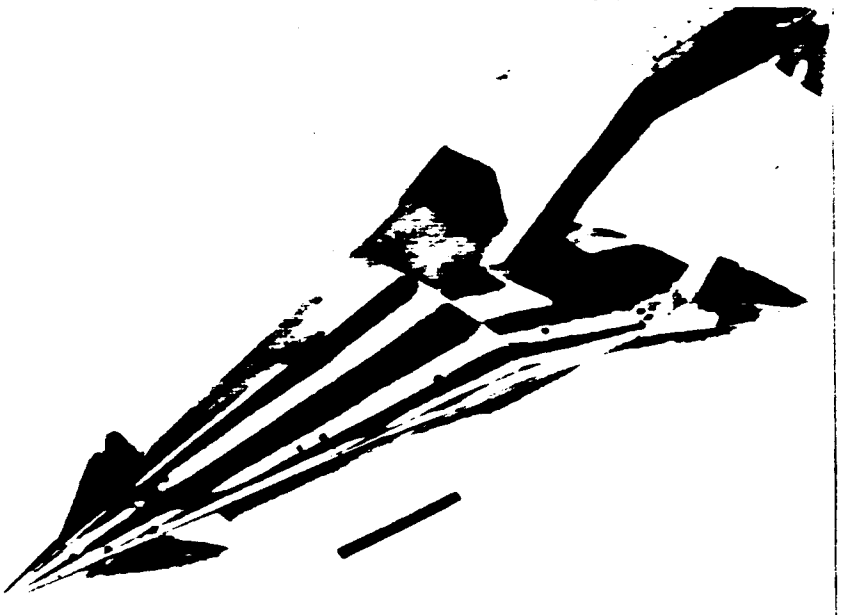

UNCLASSIFIED

AMES ALL-BODY HYPERSONIC AIRCRAFT MODEL (U)
W/O CONTROL SURFACES (U)

(U) This is a sketch of the all-body model without control surfaces to show the basic model geometry and dimensions. As previously stated, the model is 3-ft long and has a delta planform with 75° sweepback and elliptical cross sections for both the forebody and afterbody. The juncture between the forebody and afterbody occurs at 2/3 of the body length. The model nose can be either sharp or blunt with the blunt nose blended smoothly into elliptical shape of body. At the vertical symmetry plane, the elliptic-cone forebody has a half angle of only 3.83°, while the elliptic afterbody has a half angle of 7.63°.

ALL–BODY HYPERSONIC AIRCRAFT MODEL (U)
W/O CONTROL SURFACES (U)

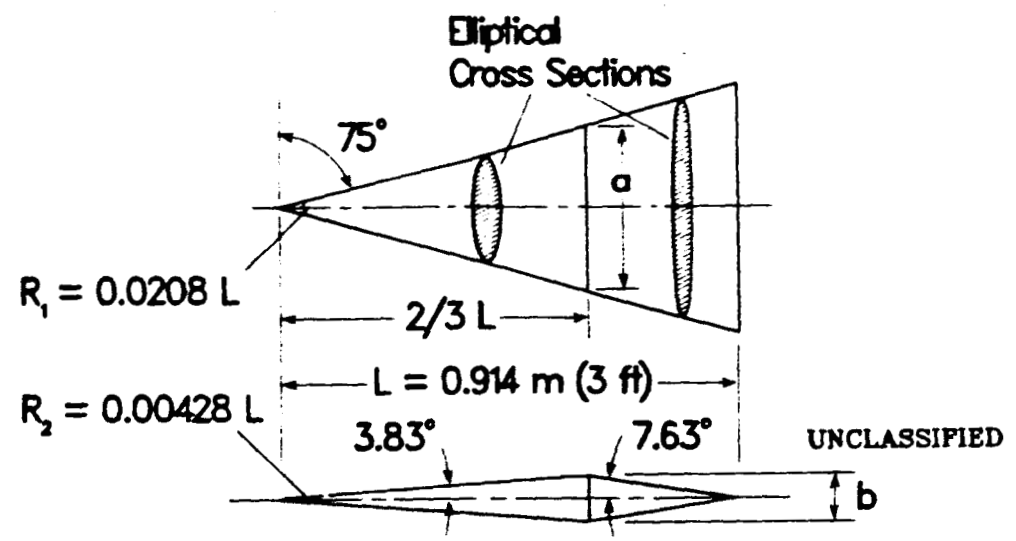

(U) Forebody – Elliptic Cone (a/b = 4) with Sharp or Blunt Nose Tip
Afterbody – Elliptical Cross Sections with Sharp Trailing Edge

AMES ALL-BODY HYPERSONIC AIRCRAFT MODEL IN NASA/AMES 3.5-FT HWT (U)

W/O CONTROL SURFACES; LENGTH = 3 FT (U)

(U) This is a photograph of the all-body model without control surfaces installed in the NASA/Ames 3.5-foot Hypersonic Wind Tunnel. A segment of the circular nozzle exit for the tunnel can be seen ahead of the model. The model support sting exits the top surface of the model afterbody.

ORIGINAL PAGE IS
OF POOR QUALITY

ALL–BODY HYPERSONIC AIRCRAFT MODEL
IN NASA/AMES 3.5–FT HWT (U)
W/O CONTROL SURFACES; LENGTH = 3 FT (U)

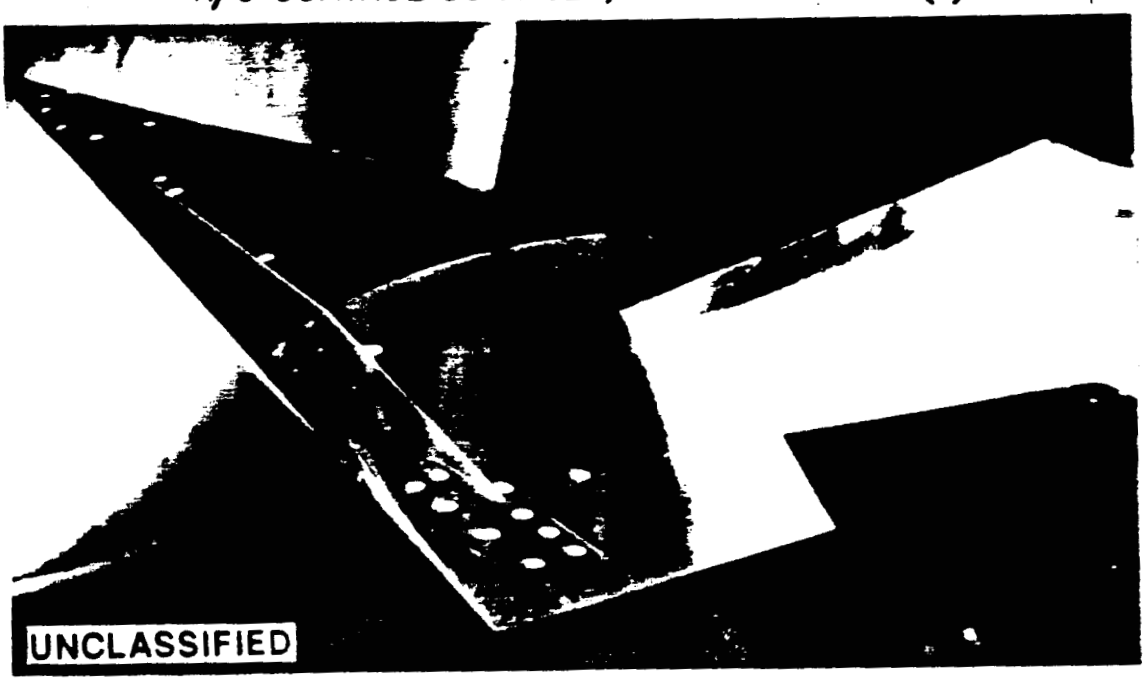

6–5

AMES ALL-BODY HYPERSONIC AIRCRAFT EXPERIMENT (U)

AMES 3.5-FT HWT (U)

(U) The Ames 3.5-foot Hypersonic Wind Tunnel (ref. 6) is a closed-circuit, blowdown-type tunnel with a pebble-bed heater to heat the air to prevent liquefaction and with axisymmetric contoured nozzles to achieve the test Mach numbers. The tunnel is equipped with a model quick-insert mechanism for quickly moving models (transit time as short as 1/2 sec) into and out of the air stream.

(U) The test conditions for this study will include nominal free-stream Mach numbers of 5, 7, and 10 (Mach 14 nozzle being redesigned.); free-stream Reynolds numbers, based on model length of 3 ft, from 1.5×10^6 to 25×10^6 (laminar to turbulent flows); and model angles of attack of 0°, 5°, 10°, and 15° (attached and separated flows). For the complete investigation, flow-visualization data (shadowgraphs and surface oil-flow patterns), surface pressures, surface heat transfer, and flow-field surveys (probes and laser velocimetry) will be obtained for the all-body model both without and with control surfaces (combination horizontal/vertical tails).

(U) As previously stated, results from the flow-visualization portion of the investigation will be presented in this paper. These will include shadowgraphs and oil-flow patterns for the basic all-body model without control surfaces and with both sharp and blunt nose tips. Results are presented for α = 0° and 15° to illustrate the range of flow features. The surface skin-friction lines from oil-flow patterns, along with surface heat transfer and flow-field surveys, are critical for viscous code validation.

AMES ALL-BODY HYPERSONIC AIRCRAFT EXPERIMENT (U)

AMES 3.5-FT HWT (U)

(U) TEST CONDITIONS:

- M_∞ = 5, 7, & 10 (14, if nozzle available)
- $Re_{\infty,L}$ = 1.5x10^6 to 25x10^6 (Laminar to Turbulent)
- α = 0° to 15° (Attached & Separated Flows)

(U) MEASUREMENTS:

- FLOW VISUALIZATION
  - Shadowgraphs
  - Surface Oil-Flow Patterns (Skin-Friction Lines)
- MEAN SURFACE PRESSURES
- SURFACE HEAT TRANSFER (Selected Areas)
- FLOW-FIELD SURVEYS
  - Probes (Pitot Pressure)
  - Laser Doppler Velocimetry
    - Mean Velocities
    - Turbulence Quantities

FLOW CONDITIONS FOR ALL-BODY MODEL (U)

AMES 3.5-FT HWT; MODEL LENGTH, L = 3 FT (U)

(U) For this test program, the minimum-to-maximum ranges of free-stream Reynolds numbers, $Re_{\infty,L}$, based on model length of 3 ft, are shown on this graph for the various free-stream Mach numbers, M_∞. The $Re_{\infty,L}$ ranges are 3.5×10^6 to 15×10^6, 1.5×10^6 to 25×10^6, and 1.5×10^6 to 5×10^6 at M_∞ values of 5.3, 7.4, and 10.3; respectively. At $M_\infty = 14$, when nozzle is operational, $Re_{\infty,L}$ will be limited to approximately 0.8×10^6 due to present restrictions on total pressure and temperature. The major portion of the test program is being conducted at $M_\infty = 7.4$ where there is the largest $Re_{\infty,L}$ range. For the flow-visualization results to date, $Re_{\infty,L}$ was 15×10^6 for $M_\infty = 5.3$ and $M_\infty = 7.4$, and 5×10^6 for $M_\infty = 10.3$. The windward boundary layer should be turbulent over most of the model length at $Re_{\infty,L} = 15 \times 10^6$ but may be transitional at $M_\infty = 10.3$ for $Re_{\infty,L} = 5 \times 10^6$. Boundary-layer transition studies using heat-transfer gages will be conducted to assess these assumptions.

(U) For computing the tunnel flow conditions, the air is treated as a thermally perfect, calorically imperfect gas with the relatively small imperfect-gas effects accounted for by the analysis of reference 7. Keyes' equation for viscosity (see ref. 8), rather than Sutherland's equation (ref. 7), is used because of the low free-stream static temperatures (approx 100° R).

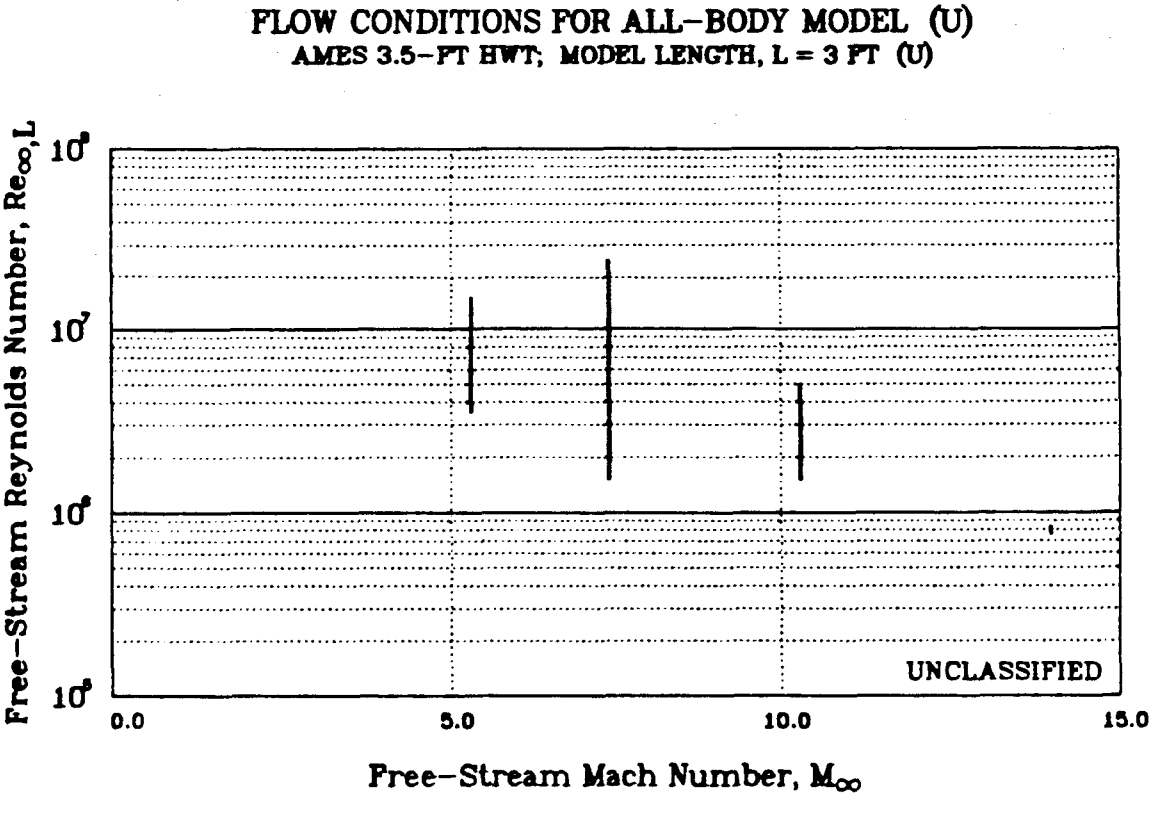

UPWIND PARABOLIZED NAVIER-STOKES CODE (U)

(U) Comparisons of the experimental results with computational results from an upwind parabolized Navier-Stokes code will be shown later. The features of this new code (ref. 9) will now be briefly described in the following figures.

(U) The upwind parabolized Navier-Stokes solver (UPS) has been developed in an effort to combine the shock-capturing characteristics of upwind numerical algorithms with the computational efficiency of a space-marching procedure. Conventional methods for solving the PNS equations incorporate artificial dissipation models which are not sufficiently adaptive to the sharp variations in flow properties associated with strong shock waves. As a result, captured shocks are generally accompanied by nonphysical oscillations and/or are smeared excessively. Recent work with algorithms for the unsteady Euler and Navier-Stokes equations has developed methods which possess inherent dissipation that is sufficiently adaptive to rapid property variations to allow the capture of extremely strong shocks without smearing or spurious oscillations. The algorithm used in the UPS code is an adaptation to the PNS equations of one of these methods.

UPWIND PARABOLIZED NAVIER–STOKES CODE (U)

(U) OBJECTIVE: DEVELOP SPACE–MARCHING FLOW SOLVER WITH IMPROVED SHOCK–CAPTURING CHARACTERISTICS FOR EFFICIENT AND ACCURATE SIMULATION OF SUPERSONIC AND HYPERSONIC VISCOUS FLOWFIELDS

(U) MOTIVATION: NUMERICAL ALGORITHMS CURRENTLY EMPLOYED IN SPACE MARCHING APPLICATIONS HAVE DIFFICULTY RESOLVING THE STRONG DISCONTINUITIES CHARACTERISTIC OF HYPERSONIC FLOW

(U) APPROACH: MODIFICATION OF A STATE–OF–THE–ART UPWIND ALGORITHM FOR USE IN INTEGRATING PARABOLIZED NAVIER–STOKES EQUATIONS

PARABOLIZED NAVIER-STOKES EQUATIONS (U)

(U) The assumptions made in deriving the parabolized Navier-Stokes equations from the unsteady Navier-Stokes equations are: 1) flow is steady, 2) streamwise viscous derivatives are small relative to those in the crossflow directions, and 3) the streamwise pressure gradient is not large. The second assumption is generally considered valid for high Reynolds number flows. The third assumption results from the neglect of part of the streamwise pressure gradient in the subsonic region of the boundary layer, which is necessary to prevent the numerical difficulties associated with the upstream propagation of information.

(U) Under the above assumptions, the governing equations are hyperbolic-parabolic with respect to the streamwise direction provided that the flow outside the boundary layer is supersonic and that no streamwise separation regions – crossflow separation does not present any numerical difficulty – are encountered. The hyperbolic-parabolic character allows numerical solution of the equations by space-marching, which is generally a considerably more efficient method for obtaining a solution in terms of both CPU time and storage requirements than is time relaxation.

PARABOLIZED NAVIER–STOKES EQUATIONS (U)

(U) PHYSICAL ASSUMPTIONS:
- Steady flow
- Negligible streamwise viscous derivatives
- Small–to–moderate streamwise pressure gradient

(U) ADVANTAGE:
- Character of equations allows space–marching solution procedure

(U) LIMITATIONS:
- Inviscid flow must be supersonic
- Flow must remain attached in streamwise direction

UPWIND PNS CODE (U)

(U) The UPS code employs a numerical algorithm which is second-order accurate and upwind in the crossflow directions. The improved shock-capturing characteristics of the algorithm are due in large part to the upwinding. Presently, the algorithm is first-order accurate in the streamwise direction. The algorithm is implicit both in the interior of the flow field and in the treatment of the boundaries. Finally, the method makes use of the finite-volume approach in order to ensure that fluxes are treated in a conservative manner.

(U) The dissipation of upwind methods allows shock waves to be sharply captured without introducing the oscillations that are typically obtained using conventional central-differencing schemes. Also, because the dissipation is inherent within the algorithm, it is not necessary for the user to specify the values of smoothing parameters.

(U) At the present stage in the code development, there is no capability for modeling the effects of turbulence or real gases; however, a simple turbulence model and equilibrium air effects are expected to be incorporated in the near future.

UPWIND PNS CODE (U)

(U) CHARACTERISTICS OF ALGORITHM:
- Second–order accurate and upwind in crossflow directions
- First–order accurate in streamwise (marching) direction
- Implicit
- Finite volume

(U) ADVANTAGES OF UPWIND SCHEMES:
- Shock waves are captured sharply and without oscillation
- User specification of smoothing parameters is not required

(U) PRESENT ASSUMPTIONS:
- Laminar flow
- Perfect gas

ALL-BODY MODEL SHADOWGRAPH (U)

$\alpha = 0^c$; SHARP NOSE (U)

$M_\infty = 7.4$; $Re_{\infty,L} = 15 \times 10^6$ (U)

(U) The next several figures illustrate the flow features for the sharp nose model. The straight bow shock, forebody boundary layer, and Prandtl-Meyer expansion at the forebody/afterbody juncture in the vertical symmetry plane are visible in this shadowgraph at $\alpha = 0^c$. The boundary layer appears to be turbulent with a thickness of approximately 1/4-in. at the juncture point.

ALL-BODY MODEL SHADOWGRAPH (U)

$\alpha = 0°$; SHARP NOSE (U)

$M_\infty = 7.4$; $Re_{\infty,L} = 15 \times 10^6$ (U)

6-11

PNS LAMINAR SOLUTION FOR ALL-BODY MODEL PRESSURE CONTOURS (U)

$\alpha = 0°$; SHARP NOSE (U)

$M_\infty = 7.4$; $Re_{\infty,L} = 15 \times 10^6$ (U)

(U) A laminar flow-field solution, using the PNS code previously described, is given here in the symmetry plane for the all-body model at the same test conditions as for the shadowgraph in the previous figure. The computed pressure contours illustrate the basic flow features, such as the bow shock and Prandtl-Meyer expansion at the forebody/afterbody juncture. As would be expected, the shock position is computed quite accurately by the code. However, this laminar computation gives a thinner boundary-layer thickness than that for the turbulent result of the experiment. Also, since the current version of the code is for laminar flow only, the surface skin-friction lines for the turbulent flow on the model were not computed.

(U) The grid used for this calculation contained 60 cells circumferentially and 43 cells stretched outward from the wall. The initial conditions required for the space-marching approach were provided by results of an iterative step-back procedure, which generated a conically similar starting solution at $x = 0.24$ m ($x/L = 0.26$). Contours between the nose and $x = 0.24$ m have been drawn by assuming the flow is conical in this region. The generation of the starting solution required approximately 40 min of CPU time on the Cray X-MP computer. The generation of the remainder of the flow field, using the space-marching technique, required approximately 1 hr of CPU time.

PNS LAMINAR SOLUTION FOR ALL-BODY MODEL PRESSURE CONTOURS (U)

$\alpha = 0°$; SHARP NOSE (U)

$M_\infty = 7.4$; $Re_{\infty L} = 15 \times 10^6$ (U)

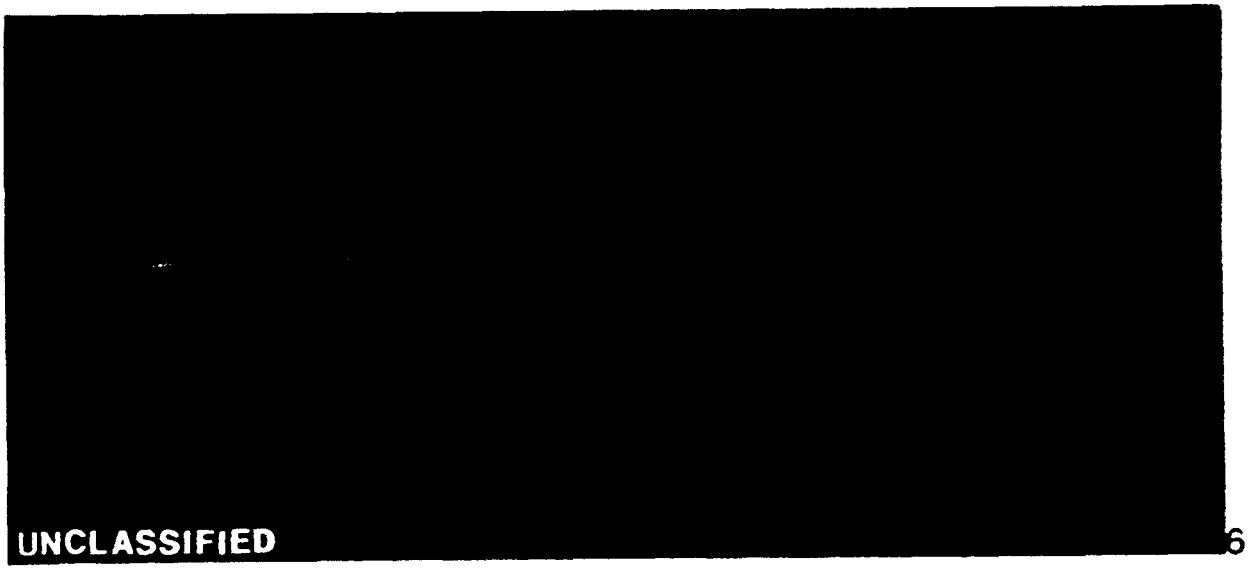

ALL-BODY MODEL SHADOWGRAPH (U)

$\alpha = 15°$; SHARP NOSE (U)

$M_\infty = 7.4$: $Re_{\infty,L} = 15 \times 10^6$ (U)

(U) The windward bow shock, forebody boundary layer, and Prandtl-Meyer expansion at the forebody/afterbody juncture are visible in this shadowgraph at $\alpha = 15°$ for the sharp nose model. As for $\alpha = 0°$, the boundary layer appears to be turbulent, but somewhat thinner.

ALL-BODY MODEL SHADOWGRAPH (U)

$\alpha = 15°$; SHARP NOSE (U)

$M_\infty = 7.4$; $Re_{\infty,L} = 15 \times 10^6$ (U)

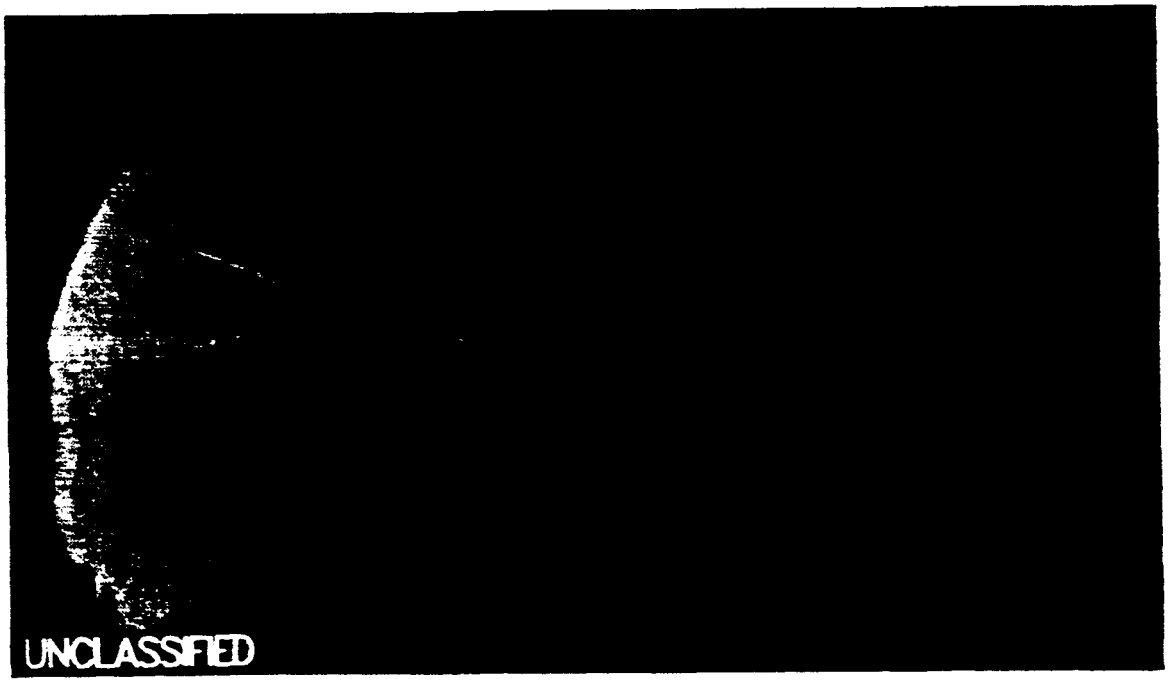

6-13

FOREBODY SHOCK-WAVE ANGLE FOR ALL-BODY MODEL (U)

SHARP NOSE; $M_\infty = 7.4$; $Re_{\infty,L} = 15 \times 10^6$ (U)

(U) This is a graph at $M_\infty = 7.4$ of the forebody shock-wave angle, Θ_w, as a function of the lower-surface inclination angle, Θ_s, for the vertical symmetry plane of the sharp nose model. As shown on the model sketch, these angles are measured from the horizontal free-stream flow direction. The value for Θ_s is the sum of the angle of attack, α, and the forebody half angle of 3.83°. Experimental values of Θ_w for $\alpha = 0°$, 5°, 10°, and 15° ($\Theta_s = 3.83°$, 8.83°, 13.83°, and 18.83°; repectively) are plotted. Also plotted are Θ_w values computed by the PNS laminar code for $\alpha = 0°$ and 10° ($\Theta_s = 3.83°$ and 13.83°, respectively). As would be expected, the PNS results are in excellent agreement with the shock-wave data. In addition, estimates of Θ_w by simple tangent-cone and tangent-wedge inviscid methods are shown. Comparing the data and PNS results to these approximate methods indicates a change from a wedge-like shock to a conical shock with increasing angle of attack (increasing Θ_s). Similar trends were observed for $M_\infty = 5.3$ and 10.3.

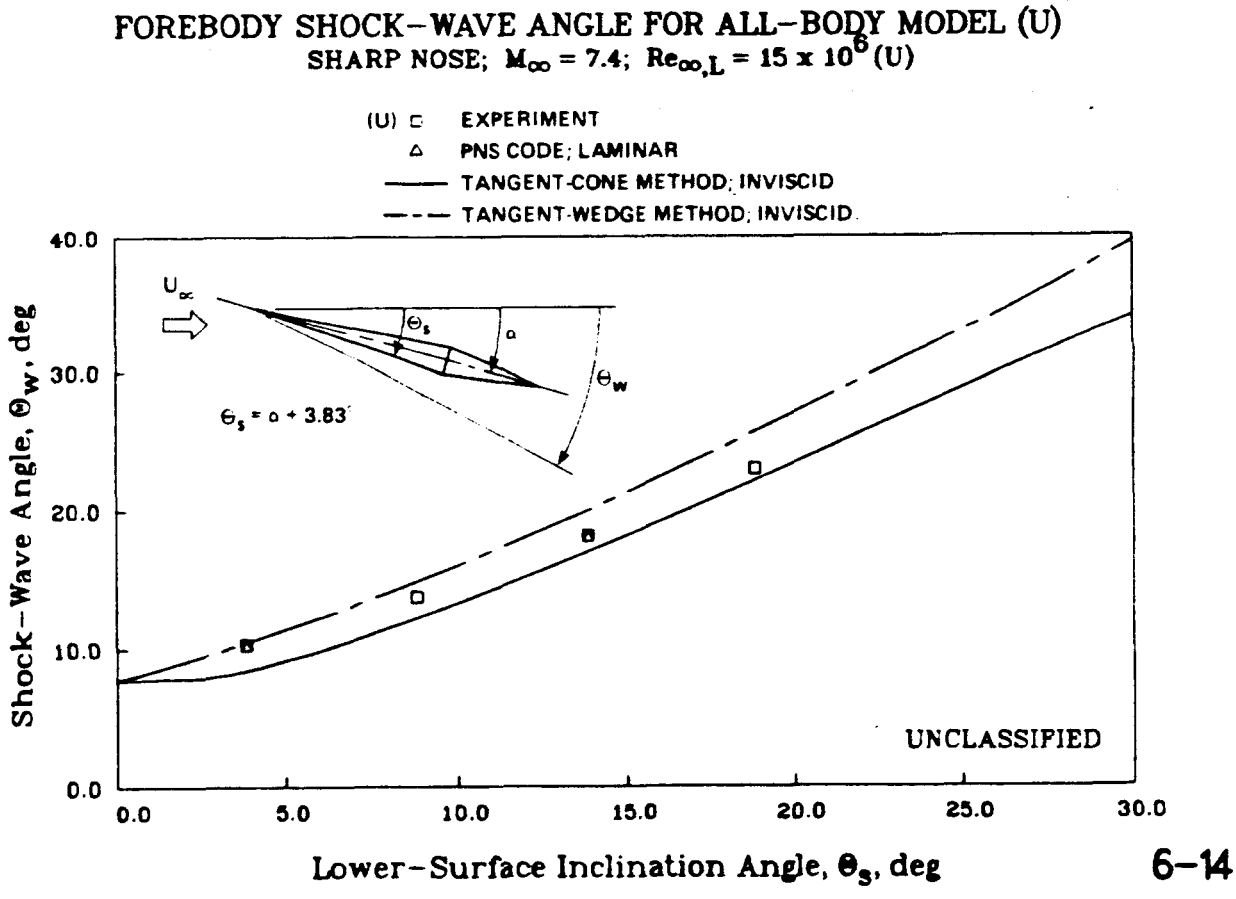

ALL-BODY MODEL OIL-FLOW PATTERN (U)

$\alpha = 0°$; SHARP NOSE (U)

$M_\infty = 7.4$; $Re_{\infty,L} = 15 \times 10^6$ (U)

(U) The skin-friction lines (limiting streamlines) were visualized using the surface oil-flow technique (ref. 10). The model was painted with a thin layer of high-temperature, flat-black paint; wet sanded; and then coated uniformly with a white oil mixture (vacuum pump oil, titanium dioxide powder, and oleic acid) to provide good contrast for photographs. The model was exposed to the tunnel flow for appoximately 10 to 30 sec, depending on test conditions, to develop a stable oil-flow pattern. During the runs, observations of the model with a video camera demonstrated that the model travel through the tunnel free-jet shear layer during model insertion and retraction had no adverse effects on the flow patterns developed during the runs. Postrun still photographs were made of the surface oil-flow patterns.

(U) The oil-flow pattern given here at $\alpha = 0°$ for the sharp nose model shows a wedge-like (strip) surface flow for the forebody. This was characteristic of the flows at all three Mach numbers. The curved line of oil-flow termination on the afterbody does not necessarily indicate flow separation, but rather lack of a fully-developed oil-flow pattern with time. A less viscous oil mixture or discrete oil dots on the model surface is required to obtain more detail in these low shear areas. This will be done in follow-on tests.

ALL–BODY MODEL OIL–FLOW PATTERN (U)

$\alpha = 0°$; SHARP NOSE (U)

$M_\infty = 7.4$; $Re_{\infty,L} = 15 \times 10^6$ (U)

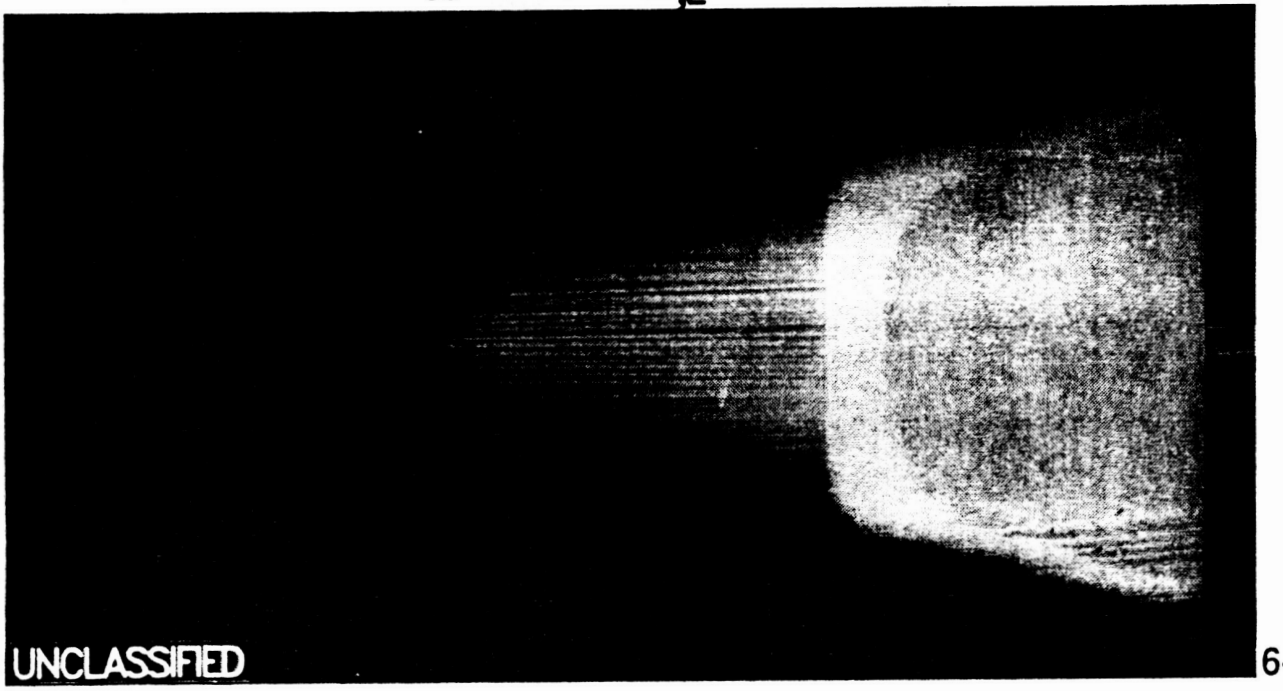

6-15

ALL-BODY MODEL OIL-FLOW PATTERN (U)

$\alpha = 15°$; WINDWARD; SHARP NOSE (U)

$M_\infty = 7.4$; $Re_{\infty,L} = 15 \times 10^6$ (U)

(U) As the angle of attack was increased for the sharp nose model, the windward oil-flow patterns changed from wedge-like (strip) to conical flow patterns. For this oil-flow photograph at angle of attack, the conical pattern of the skin-friction lines is readily visible on the windward surface of the model forebody. However, the skin-friction lines begin to converge inward toward the model centerline at the forebody/afterbody juncture. These features were characteristic of the flows at all three Mach numbers for the sharp nose model.

ALL–BODY MODEL OIL–FLOW PATTERN (U)

$\alpha = 15°$; WINDWARD; SHARP NOSE (U)

$M_\infty = 7.4$; $Re_{\infty,L} = 15 \times 10^6$ (U)

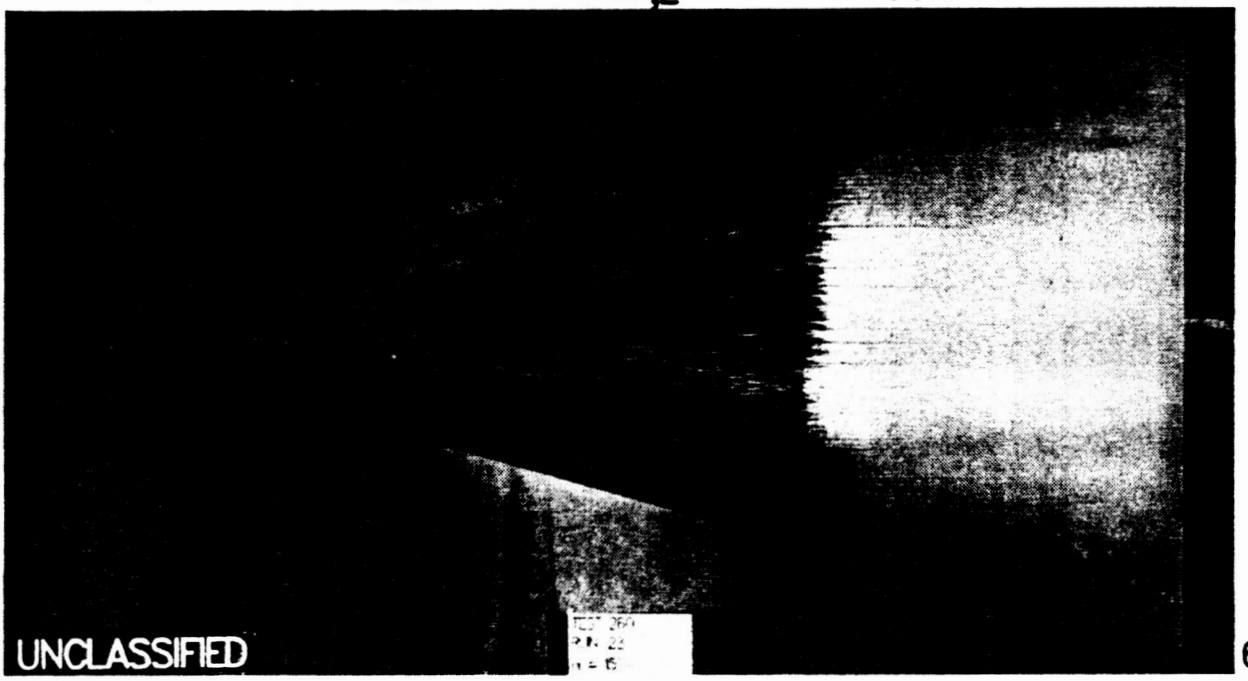

6-16

ALL-BODY MODEL OIL-FLOW PATTERN (U)

$\alpha = 15°$; LEEWARD; SHARP NOSE (U)

$M_\infty = 5.3$; $Re_{\infty,L} = 15 \times 10^6$ (U)

(U) The next three figures show leeward oil-flow patterns at $\alpha = 15°$ for $M_\infty = 5.3$, 7.4, and 10.3. This oil-flow pattern at $M_\infty = 5.3$ illustrates the complex leeward vortical flows characteristic of conical and delta-planform bodies at angle of attack. The reattachment line ("feathered" oil-flow pattern) for the two primary vortices is readily visible on the most leeward ray. The presence of two secondary vortices is also visible outboard of the primary reattachment region. The actual separation lines for the primary vortices near the model leading edges are not definitive because the oil-flow pattern may not be fully developed with time in these regions. The slight disturbances in the oil-flow pattern near the nose tip are due to transverse joints in model surface. The two straight lines along conical rays, just inboard from each leading edge, are joints for the removable cover plate on leeward surface. The shock/boundary-layer interaction at the sting attachment on the afterbody can be seen. No other significant details are apparent in the oil-flow pattern for the low-shear regions of the afterbody.

ALL–BODY MODEL OIL–FLOW PATTERN (U)

$\alpha = 15°$; LEEWARD; SHARP NOSE (U)

$M_\infty = 5.3$; $Re_{\infty,L} = 15 \times 10^6$ (U)

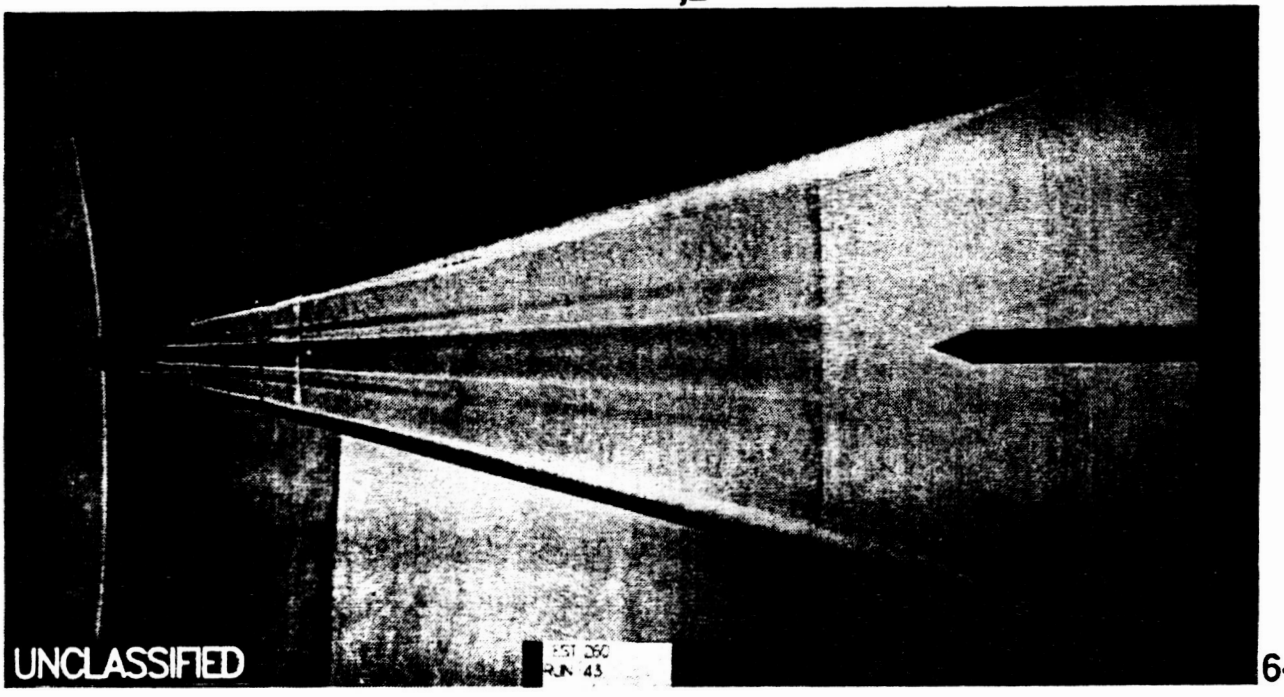

6-17

ALL-BODY MODEL OIL-FLOW PATTERN (U)

$\alpha = 15°$; LEEWARD; SHARP NOSE (U)

$M_\infty = 7.4$; $Re_{\infty,L} = 15 \times 10^6$ (U)

(U) This leeward oil-flow pattern at $M_\infty = 7.4$ is similar to that for $M_\infty = 5.3$ but the lateral extent of the primary and secondary vortices on the surface is diminished.

ALL–BODY MODEL OIL–FLOW PATTERN (U)

$\alpha = 15°$; LEEWARD; SHARP NOSE (U)

$M_\infty = 7.4$; $Re_{\infty,L} = 15 \times 10^6$ (U)

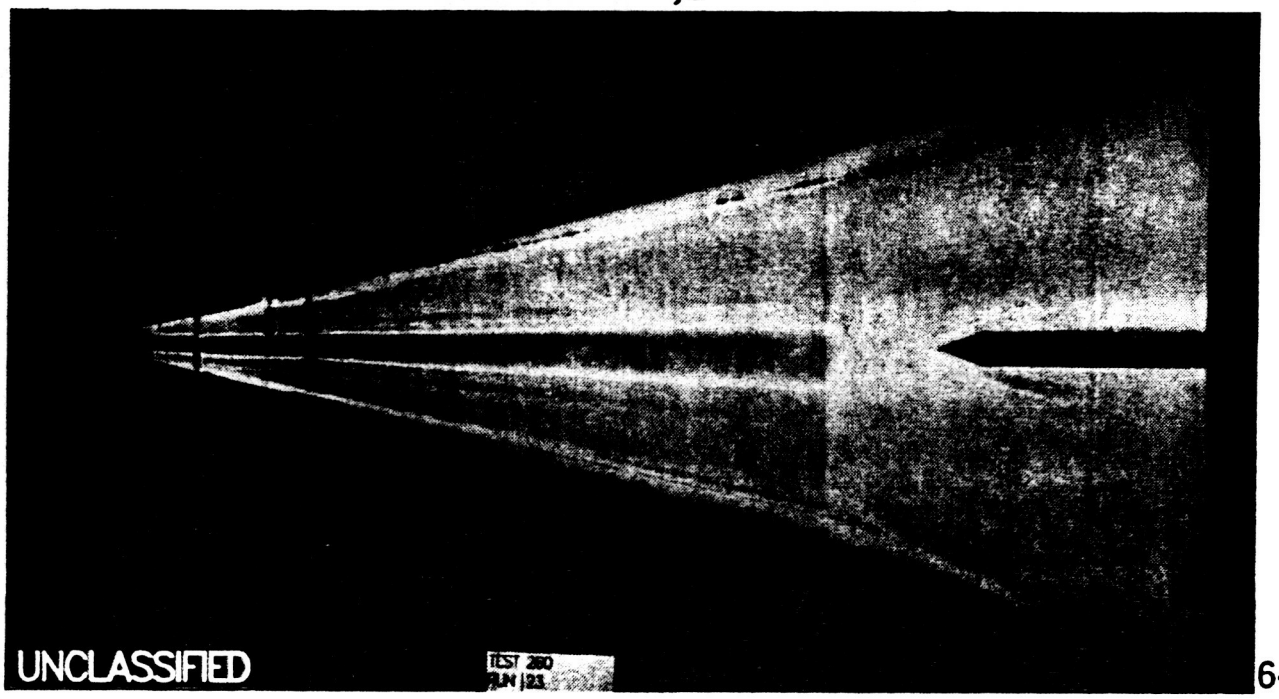

6-18

ALL-BODY MODEL OIL-FLOW PATTERN (U)

$\alpha = 15°$; LEEWARD; SHARP NOSE (U)

$M_\infty = 10.3$; $Re_{\infty,L} = 5 \times 10^6$ (U)

(U) This leeward oil-flow pattern at $M_\infty = 10.3$ shows still less extent of the reattachment region for the primary vortices compared to the previous results for $M_\infty = 5.3$ and 7.4. Also, no secondary vortices are evident on the surface from this oil-flow pattern. The last three leeward oil-flow patterns illustrate a diminishing extent of the vortical surface patterns with increasing Mach number. Some of the effects observed at $M_\infty = 10.3$ could also be due to a lower Reynolds number than that for $M_\infty = 5.3$ and 7.4 (5×10^6 vs 15×10^6).

ALL–BODY MODEL OIL–FLOW PATTERN (U)

$\alpha = 15°$; LEEWARD; SHARP NOSE (U)

$M_\infty = 10.3$; $Re_{\infty,L} = 5 \times 10^6$ (U)

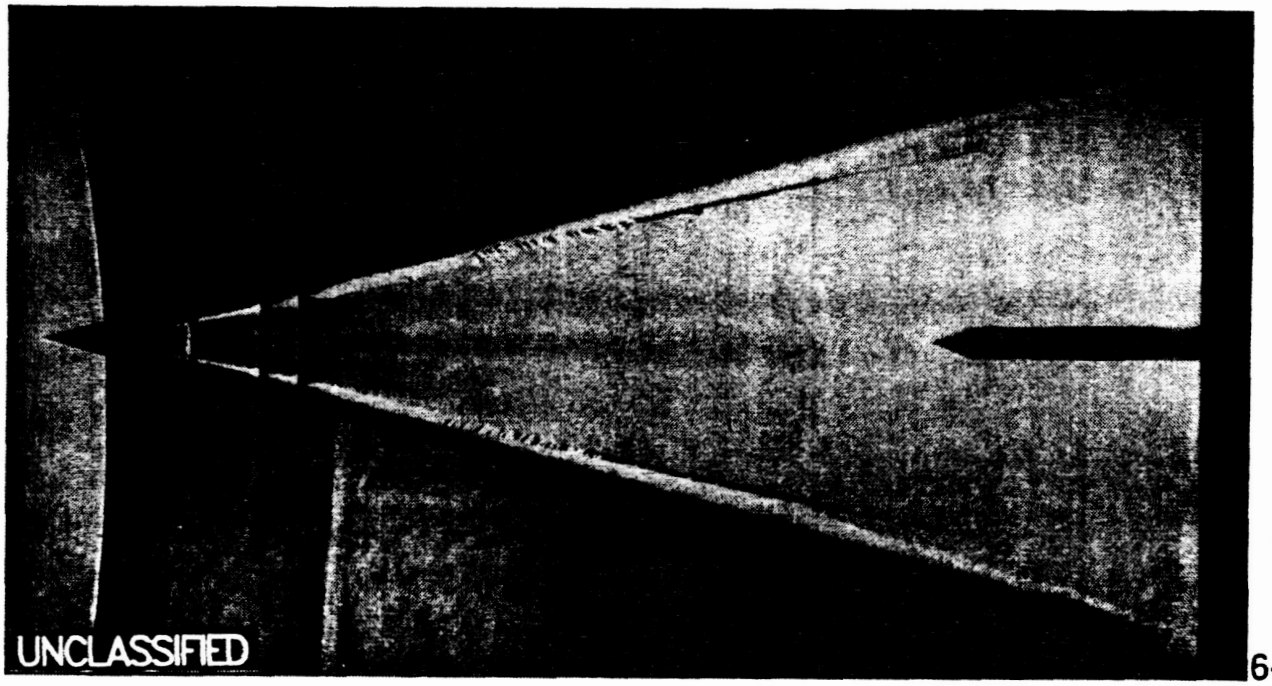

6-19

ALL-BODY MODEL SHADOWGRAPH (U)

$\alpha = 0^{\circ}$; BLUNT NOSE (U)

$M_{\infty} = 7.4$; $Re_{\infty,L} = 15 \times 10^{6}$ (U)

(U) The next several figures illustrate the flow features for the blunt nose model at $M_{\infty} = 7.4$ and $Re_{\infty,L} = 15 \times 10^{6}$. The curved bow shock and the Prandtl-Meyer expansion at the forebody/afterbody juncture are visible in this shadowgraph at $\alpha = 0^{\circ}$. The forebody boundary layer, unlike for the sharp nose model, is not evident in the shadowgraph.

ALL-BODY MODEL SHADOWGRAPH (U)

$\alpha = 0^{\circ}$; BLUNT NOSE (U)

$M_{\infty} = 7.4$; $Re_{\infty,L} = 15 \times 10^{6}$ (U)

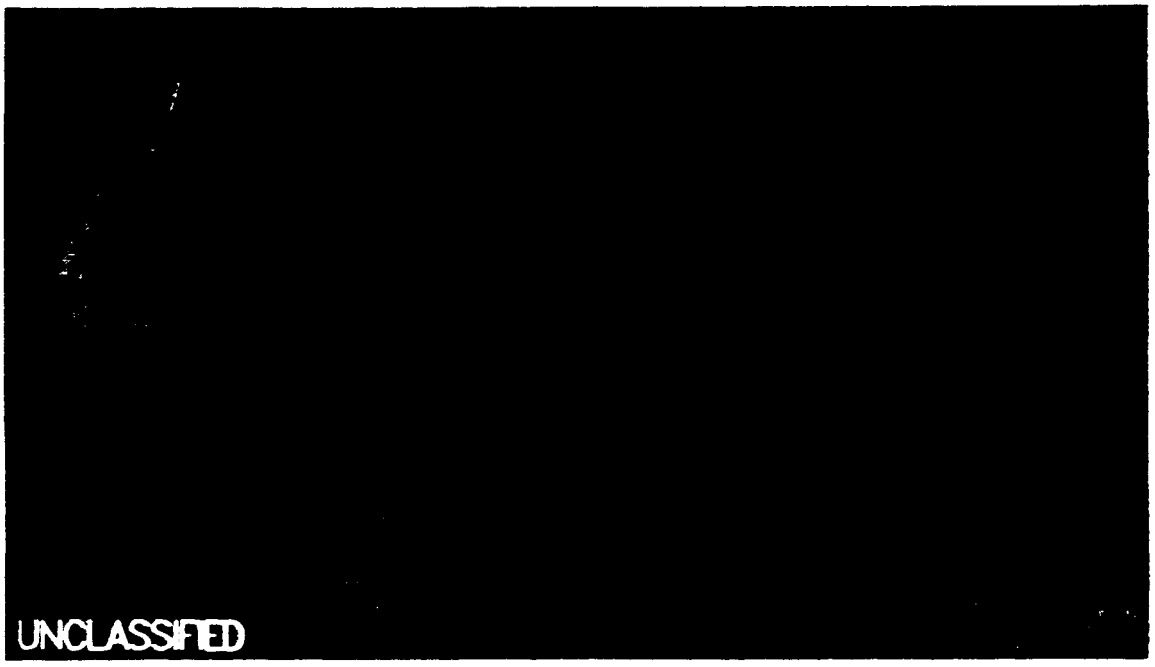

6-20

ALL-BODY MODEL SHADOWGRAPH (U)

$\alpha = 15^{\circ}$; BLUNT NOSE (U)

$M_{\infty} = 7.4$; $Re_{\infty,L} = 15 \times 10^{6}$ (U)

(U) The bow shock is observed on both the windward and leeward sides of the blunt nose model in this shadowgraph at $\alpha = 15^{\circ}$. The forebody boundary layer and the Prandtl-Meyer expansion at the forebody afterbody juncture are also visible on the windward side.

ALL-BODY MODEL SHADOWGRAPH (U)

$\alpha = 15^{\circ}$; BLUNT NOSE (U)

$M_{\infty} = 7.4$; $Re_{\infty,L} = 15 \times 10^{6}$ (U)

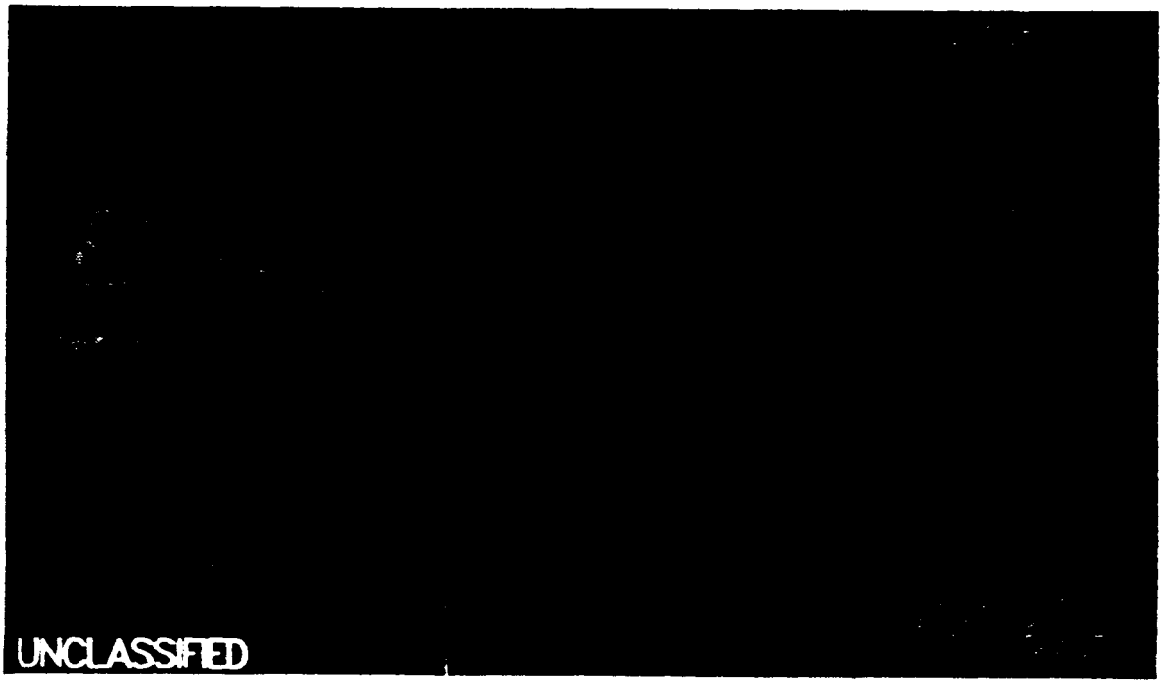

6-21

ALL-BODY MODEL OIL-FLOW PATTERN (U)

$\alpha = 0°$; BLUNT NOSE (U)

$M_\infty = 7.4$; $Re_{\infty,L} = 15 \times 10^6$ (U)

(U) The oil-flow pattern, given here at $\alpha = 0°$ for the blunt nose model, shows the surface skin-friction lines converging on the forebody toward the model centerline. This is a departure from the strip-type flow observed with the sharp nose model at $\alpha = 0°$. Just downstream of the blunt nose there is also a low shear region with possible flow separation. As for the sharp nose model, the curved line of oil-flow termination on the afterbody does not necessarily indicate flow separation, but rather lack of a fully-developed oil-flow pattern with time.

ALL–BODY MODEL OIL–FLOW PATTERN (U)

$\alpha = 0°$; BLUNT NOSE (U)

$M_\infty = 7.4$; $Re_{\infty,L} = 15 \times 10^6$ (U)

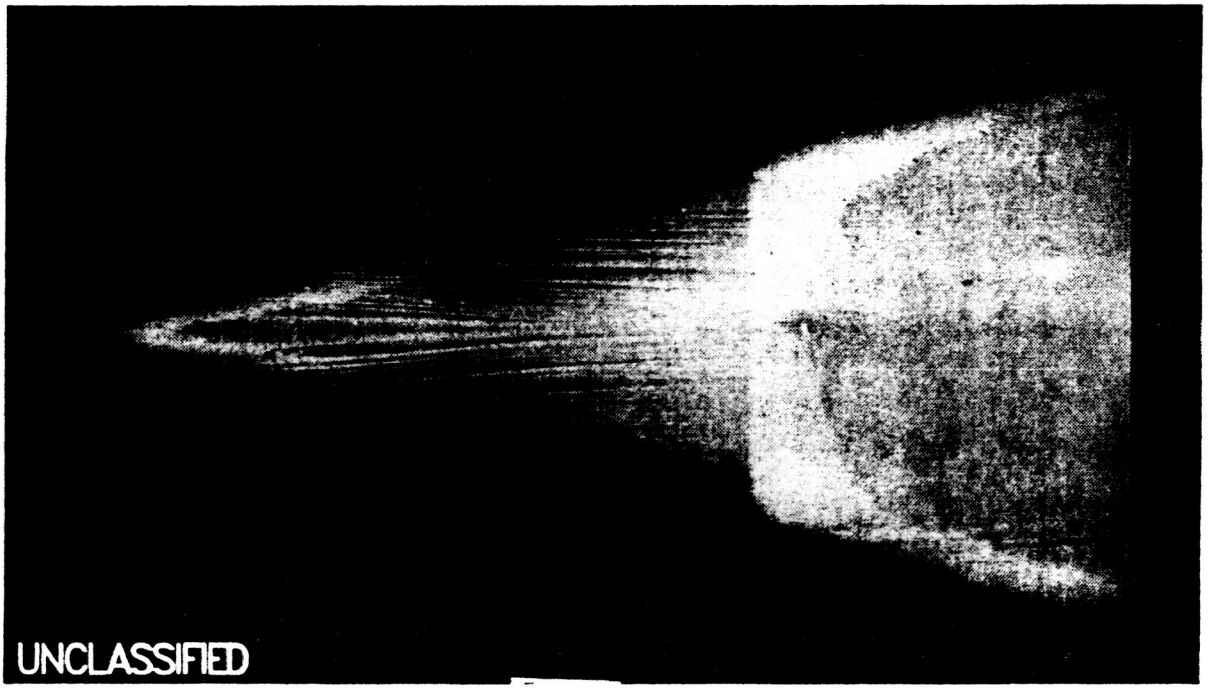

6-22

ALL-BODY MODEL OIL-FLOW PATTERN (U)

$\alpha = 15°$; WINDWARD; BLUNT NOSE (U)

$M_\infty = 7.4$; $Re_{\infty,L} = 15 \times 10^6$ (U)

(U) For this windward oil-flow pattern at $\alpha = 15°$, there is still some convergence of the skin-friction lines near the nose due to bluntness. Downstream of the bluntness effects, a conical pattern of the skin-friction lines is readily visible on the remainder of the forebody surface and, as for the sharp nose model, the skin-friction lines begin to converge inward toward the model centerline at the forebody/afterbody juncture.

ALL–BODY MODEL OIL–FLOW PATTERN (U)

α = 15°; WINDWARD; BLUNT NOSE (U)

$M_\infty = 7.4$; $Re_{\infty,L} = 15 \times 10^6$ (U)

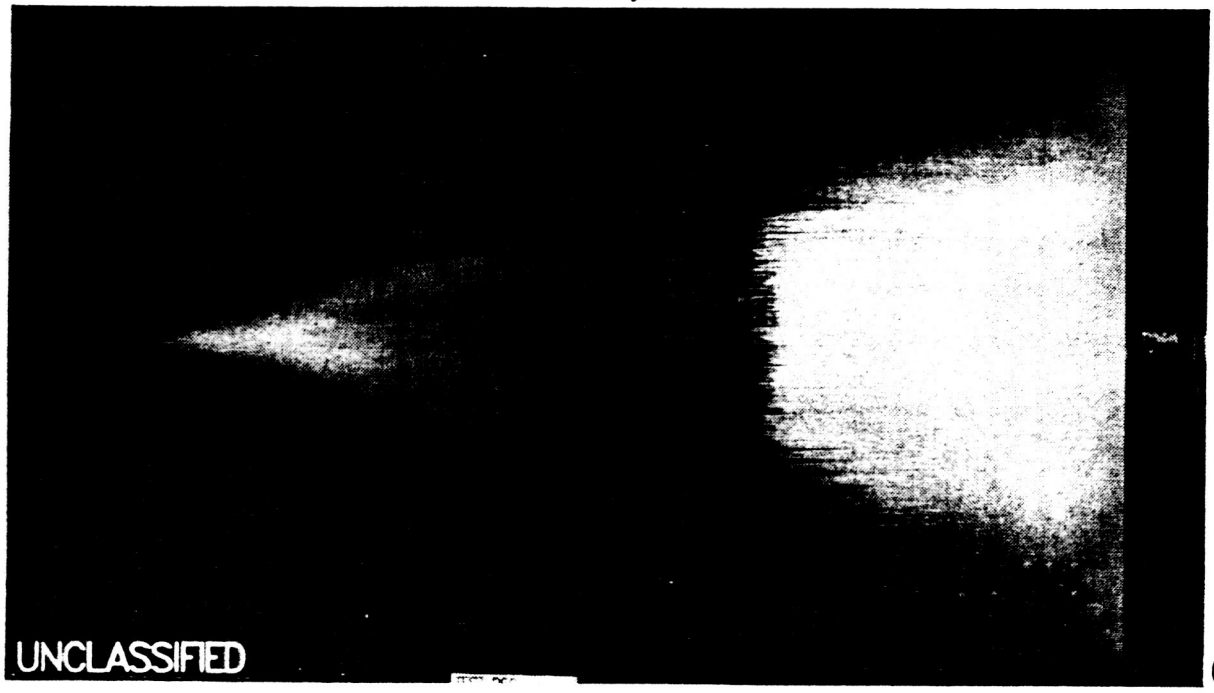

6-23

ALL-BODY MODEL OIL-FLOW PATTERN (U)

$\alpha = 15°$; LEEWARD; BLUNT NOSE (U)

$M_\infty = 7.4$; $Re_{\infty,L} = 15 \times 10^6$ (U)

(U) This leeward oil-flow pattern, corresponding to the previous windward result, illustrates the increased complexity of the leeside flow for blunt-nosed bodies compared to that for sharp-nosed bodies at angle of attack. Multiple vortical patterns are readily seen. The reattachment line ("feathered" oil-flow pattern) for the two primary vortices is visible on the most leeward ray. The presence of other vortices in the nose region due to bluntness is quite evident.

ALL–BODY MODEL OIL–FLOW PATTERN (U)

$\alpha = 15°$; LEEWARD; BLUNT NOSE (U)

$M_\infty = 7.4$; $Re_{\infty,L} = 15 \times 10^6$ (U)

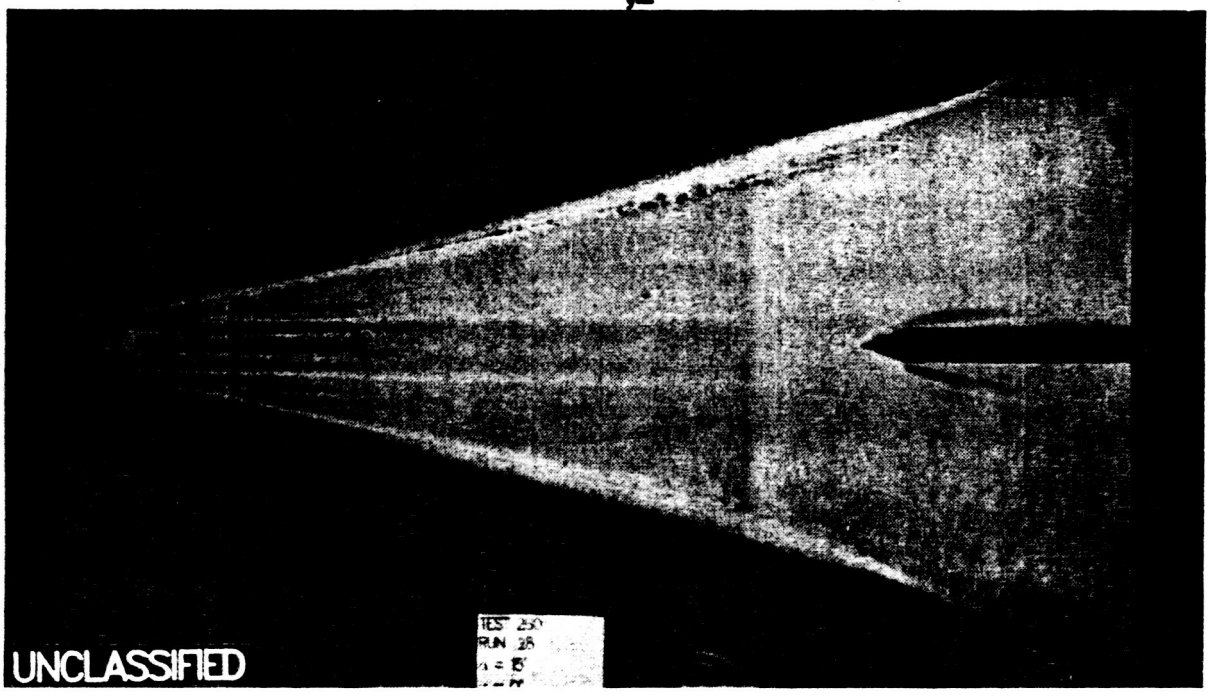

6-24

CONCLUDING REMARKS (U)

(U) This paper defined a comprehensive test program in the NASA/Ames 3.5-foot Hypersonic Wind Tunnel for obtaining data on a generic all-body hypersonic vehicle for CFD code validation, outlined the major features of a new upwind PNS code being applied to the all-body model, and presented flow-visualization results for sharp and blunt nose models at angles of attack from 0° to 15°.

CONCLUDING REMARKS (U)

(U) • DEFINED TEST PROGRAM IN AMES 3.5–FT HWT WITH ALL–BODY MODEL

(U) • OUTLINED FEATURES OF NEW UPWIND PNS CODE

(U) • PRESENTED FLOW–VISUALIZATION RESULTS
- SHARP NOSE MODEL
  - — PNS computations illustrate basic flow features and, as would be expected, are in excellent agreement with shock–wave data
  - — Windward data indicate change from wedge–like (strip) to conical forebody flow with increasing angle of attack
  - — Complex leeward separated and vortical flows at angle of attack
- BLUNT NOSE MODEL
  - — Increased complexity of both windward & leeward flows with nose bluntness

REFERENCES (U)

(U) 1. Gregory, Thomas J.; Ardema, Mark D.; and Waters, Mark H.: Hypersonic Transport Preliminary Performance Estimates for an All-Body Configuration. AIAA Paper 70-1224, Oct. 1970.

(U) 2. Williams, Louis J.: Estimated Aerodynamics of All-Body Hypersonic Aircraft Configurations. NASA TM X-2091, 1971.

(U) 3. Gregory, Thomas J.; Williams, Louis J.; and Wilcox, Darrell E.: The Airbreathing Launch Vehicle for Earth Orbit Shuttle - Performance and Operation. AIAA Paper 70-270, Feb. 1970.

(U) 4. Gregory, Thomas J.; Wilcox, Darrell E.; and Williams, Louis J.: The Effects of Propulsion System - Airframe Interactions on the Performance of Hypersonic Aircraft. AIAA Paper 67-493, July 1967.

(U) 5. Nelms, Walter P., Jr.; and Thomas, Charles L.: Aerodynamic Characteristics of an All-Body Hypersonic Aircraft Configuration at Mach Numbers from 0.65 to 10.6. NASA TN D-6577, 1971.

(U) 6. Penaranda, Frank E.; and Freda, M. Shannon; eds.: Aeronautical Facilities Catalogue, Volume I, Wind Tunnels. NASA RP-1132, 1985.

(U) 7. Ames Research Staff: Equations, Tables, and Charts for Compressible Flow. NASA TR-1135, 1953.

(U) 8. Bertram, Mitchel H.: Comment on "Viscosity of Air." J. Spacecraft & Rockets, vol. 4, no. 2, Feb. 1967, pp. 287–288.

(U) 9. Lawrence, S.; Chaussee, D. S.; and Tannehill, J. C.: Application of an Upwind Algorithm to the Three-Dimensional Parabolized Navier-Stokes Equations. AIAA Paper 87-1112, June 1987.

(U) 10. Maltby, R. L.: Flow Visualization in Wind Tunnels Using Indicators. AGARDograph 70, Apr. 1962.